

# First-principle electronic properties of dilute-P AINP deep ultraviolet semiconductor

Damir Borovac, Chee-Keong Tan, and Nelson Tansu

Citation: *AIP Advances* **8**, 085119 (2018); doi: 10.1063/1.5036978

View online: <https://doi.org/10.1063/1.5036978>

View Table of Contents: <http://aip.scitation.org/toc/adv/8/8>

Published by the [American Institute of Physics](#)

---

---

**AIP** | Conference Proceedings

Get **30% off** all  
print proceedings!

Enter Promotion Code **PDF30** at checkout



## First-principle electronic properties of dilute-P AlN<sub>1-x</sub>P<sub>x</sub> deep ultraviolet semiconductor

Damir Borovac,<sup>1,a</sup> Chee-Keong Tan,<sup>2</sup> and Nelson Tansu<sup>1,b</sup>

<sup>1</sup>Center for Photonics and Nanoelectronics, Department of Electrical and Computer Engineering, Lehigh University, Bethlehem, Pennsylvania 18015, USA

<sup>2</sup>Department of Electrical and Computer Engineering, Clarkson University, Potsdam, New York 13699, USA

(Received 19 April 2018; accepted 14 August 2018; published online 22 August 2018)

The electronic properties of dilute-P AlN<sub>1-x</sub>P<sub>x</sub> alloys are investigated by means of First-Principle Density Functional Theory (DFT) calculations, where the phosphorus (P) content is varied from 0% up to 6.25%. Band structure calculations indicate significant modifications of the electronic properties with the introduction of P-atoms, with the possibility of tuning the energy band gap from 6.19eV down to 4.32eV by inserting 6.25% P-content in the AlN-based system. The carrier effective masses and lattice parameters (*a* and *c*) were analyzed, and a large bowing parameter of  $b = 28.3 \pm 0.5$  eV was found. Moreover, our findings suggest a potential pathway to engineer the valence band crossover between the crystal-field split-off (CH) band and the heavy hole (HH) band by inserting low amounts of P-content (~1-2%) into the AlN<sub>1-x</sub>P<sub>x</sub> alloy. Thus, the dilute-P AlN<sub>1-x</sub>P<sub>x</sub> alloys may serve as potential candidates for implementation as the active region material for dominant transverse electric (TE) polarization for deep-UV emitting devices. © 2018 Author(s). All article content, except where otherwise noted, is licensed under a Creative Commons Attribution (CC BY) license (<http://creativecommons.org/licenses/by/4.0/>). <https://doi.org/10.1063/1.5036978>

### I. INTRODUCTION

The family of III-nitride semiconductors has gained tremendous attention over the course of the last few decades, primarily owing to their favorable optoelectronic, electronic, chemical and tribological material properties suitable for a wide range of applications.<sup>1-6</sup> In particular, the binary, ternary and quaternary alloys of the III-nitride semiconductor family provide access to a broad range of emission wavelengths ranging from deep ultra-violet (DUV) up to mid-infrared (IR).<sup>7</sup> Great success has been demonstrated for fabricating highly efficient light emitting diodes (LEDs) suitable for emission in the blue and violet spectral regimes, for which the breakthrough works were recognized by the Nobel Prize in Physics in 2014.<sup>8</sup> Despite the accomplishments of In<sub>x</sub>Ga<sub>1-x</sub>N-based materials for visible light applications, the Al<sub>x</sub>Ga<sub>1-x</sub>N alloys for deep-UV applications have seen much slower progress.<sup>9</sup> Enabling high-efficiency devices operating in the UV-C ( $\lambda \sim 200\text{nm} - 280\text{nm}$ ) wavelength regime is highly important for the applications of water, air and food purification, polymer curing, semiconductor photolithography and high density optical recording amongst many others.

The highest reported external quantum efficiency (EQE) of a III-nitride-based DUV emitter below  $\lambda \sim 300\text{nm}$  is currently at 20.3%, at a wavelength of 275 nm with 20 mA operating current.<sup>10</sup> In comparison to the InGaN blue LED with an EQE of ~80%, the efficiency of AlGa<sub>x</sub>N-based DUV LED is still much lower than its counterpart.<sup>11</sup> The relatively slow progress in realizing highly efficient DUV devices has been affected by several factors, including the need for transparent, low-cost and lattice-matched substrates to AlN, low p-type conductivity, low light extraction efficiency (LEE)

<sup>a</sup>Electronic mail: [dab315@lehigh.edu](mailto:dab315@lehigh.edu)

<sup>b</sup>Electronic mail: [tansu@lehigh.edu](mailto:tansu@lehigh.edu)

and others.<sup>9</sup> To mitigate these detrimental effects on the EQE, numerous active region designs have been employed, with relative success on improving the EQE in the deep-UV spectral regime.<sup>12–16</sup> Additionally, the high Al-content  $\text{Al}_x\text{Ga}_{1-x}\text{N}$  alloys suffer from a fundamental drawback arising from the valence band crossover issue, where the crystal-field split-off band resides above the heavy-hole (HH) and light-hole (LH) bands.<sup>17,18</sup> This arrangement of the top-most valence bands results in transverse magnetic (TM) dominant polarization, making it difficult to extract light out of conventional top-emitting LEDs which typically employ designs suited for extracting light in the vertical direction.<sup>19,20</sup> Therefore, pursuing research on novel III-nitride-based material platforms for applications in the DUV-regime is instrumental and can provide new opportunities for future deep-UV LED design.

Previous works on mixed-anion III-nitride semiconductors have shown that incorporating minute amounts of group-V elements (P, As, Sb or Bi) can lead to strong bowing in GaN-based alloys.<sup>21–24</sup> Prime examples of such material systems include the dilute-P GaNP and dilute-As GaNAs alloys, for which several theoretical and experimental works have been reported describing their fundamental properties and potential for active region implementation.<sup>21,25–27</sup> In particular, the dilute-As GaNAs alloys possess excellent potential for tackling the efficiency-hindering Auger recombination issue in III-nitride semiconductors due to their favorable electronic properties.<sup>28,29</sup> Similarly, recent work on the electronic properties of dilute-P GaNP alloys showed their capability for applications in the visible light regime attributed to their ability to push for longer wavelength emission.<sup>30</sup> While the dilute-anion GaN-based semiconductors have been investigated to some extent, the literature on AlN-based dilute-anion semiconductors is extremely limited.<sup>31</sup> A novel material system based on the dilute-As AlNAs alloy has recently been suggested as a new potential candidate for DUV emission due to the possibility of covering the entire UV-C ( $\lambda \sim 200\text{nm} - 290\text{nm}$ ) spectral regime, as well as its capability to suppress the valence band crossover issue.<sup>32</sup> However, literature on dilute-P AlNP has been non-existent by present. Therefore, investigating the electronic properties of the dilute-P  $\text{AlN}_{1-x}\text{P}_x$  alloys is instrumental as it may provide new pathways for applications in the DUV spectral regime by employing this III-nitride-based material system.

In this work, an analysis is presented on the electronic properties of the dilute-P AlNP alloy by using First-Principle Density Functional Theory (DFT) calculations. The nitrogen (N) atoms are replaced by phosphorus (P) atoms in the AlNP alloy and the P-content is varied from 0% up to 6.25%. The electronic band structures and electronic properties including the energy band gap, carrier effective masses and lattice parameters  $a$  and  $c$  are presented, and comparison is drawn to other III-nitride-based material systems. Moreover, the effect of the P-incorporation on the valence band crossover between the crystal-field split-off (CH) and heavy hole (HH) band in the AlN-based system is analyzed. Our findings indicate the strong potential of dilute-P  $\text{AlN}_{1-x}\text{P}_x$  alloys for implementation as the active region material in mid- and deep-UV light-emitting applications.

## II. COMPUTATIONAL METHOD

The DFT calculations for obtaining the band structures of the dilute-P AlNP alloy utilized the supercell approach for building the corresponding crystal structures. The phosphorus content is varied by substituting one nitrogen atom with one phosphorus atom at a time, while varying the supercell size. This approach has been reported in previous works.<sup>32,33</sup> As an example, figure 1 illustrates a 128-atom ( $4 \times 4 \times 2$ ) supercell consisting of 64 aluminum (Al), 63 nitrogen and one phosphorus atom, which correlates to 1.56% P-content in the  $\text{AlN}_{1-x}\text{P}_x$  alloy. The projector augmented wave (PAW) method was implemented for obtaining the band structure calculations, as implemented in the MedeA Vienna ab initio simulation package (VASP).<sup>34–37</sup> The Generalized Gradient Approximation (GGA) and the Perdew-Burke-Ernzerhof (PBE) exchange-correlation functional were used for optimizing the crystal structures, and the atoms were relaxed with the Hellman-Feynman force set to  $0.02 \text{ eV}/\text{\AA}$ .<sup>38</sup> Moreover, the cut-off energy was set to 400 eV, the energy convergence criterion was set as  $1 \times 10^{-5} \text{ eV/atom}$  and the external pressure to 0 GPa. The band structure calculations were iterated until convergence of the band gap ( $E_g$ ) values was achieved and the calculations were performed using the blocked Davidson algorithm, with the integration scheme set to the tetrahedron smearing method. Moreover, the k-meshes were varied based on the supercell size, where the 128-atom had a

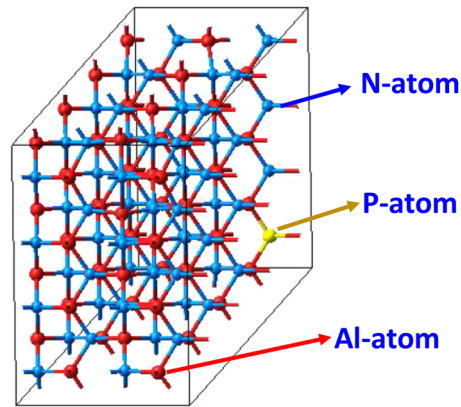


FIG. 1. An example of a 128-atom ( $4 \times 4 \times 2$ ) supercell of dilute-P AlNP, with 64 aluminum, 63 nitrogen and 1 phosphorus atom.

$4 \times 4 \times 4$  mesh and the 32-atom an  $8 \times 8 \times 4$  mesh. Thus, the spin-orbit coupling effect was not taken into account as its effect on this specific AlN-based wide band gap material system was found to be negligible.

### III. RESULTS AND DISCUSSIONS

In figures 2(a) and 2(b), the DFT-calculated band structures of AlN and AlNP alloy with 6.25% P-content are presented, respectively. It can be noted that the AlNP alloy with 6.25% P-content retains the direct band gap property, where the valence band minima (VBM) and conduction band maxima (CBM) meet at the gamma ( $\Gamma$ ) point in the reduced Brillouin Zone (BZ). The direct band gap property is an essential attribute for efficient emission in photonic device applications due to the higher probability of electrons and holes recombining in active regions of light-emitting devices. Moreover, the figures indicate large perturbations in the energy dispersion relations for the AlN-based alloy when phosphorus atoms are introduced, resulting in significant modifications of the conduction and valence band dispersions. The changes are caused by the introduction of defect P-states within the energy gap of the AlN material resulting in modifications of the band structure. Similar effects have been observed in the dilute-P GaNP alloys, where the P-impurities lead to significant reduction of the energy band gap, caused by the defect P-states in the energy gap.<sup>39</sup>

From figure 2(a) the DFT-calculated band structure of AlN indicates that the energy difference between the CBM and the VBM at the  $\Gamma$  point is  $E_g = 6.18$  eV, whereas the 6.25% P-content AlNP alloy in figure 2(b) has a value of  $E_g = 4.32$  eV. The energy band gap value for AlN is in excellent agreement with experimentally reported values for those measured at room temperature by Yim

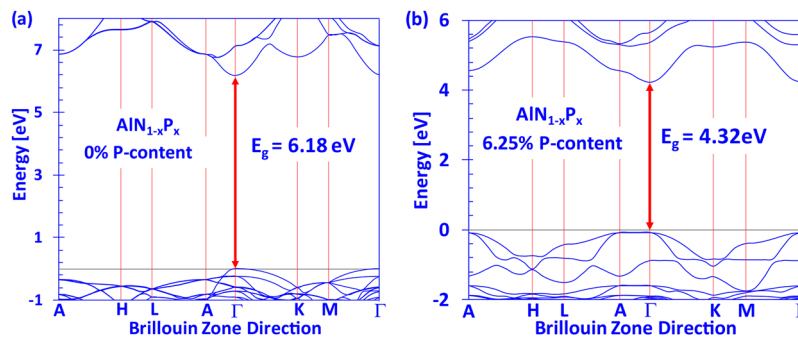


FIG. 2. a) Electronic band structure of AlN and b) AlNP, with 6.25% phosphorus content. The  $E_g$  values are taken as the difference between the conduction band minima (CBM) and valence band maxima (VBM).

and co-workers (6.2 eV).<sup>40</sup> Note that the values of the energy band gaps in figure 2(a) and 2(b) were obtained by applying a scissor operator to shift the conduction band edges by a value of 1.98 eV and 1.9 eV, respectively, in order to account for the energy band gap underestimation arising from the GGA band structure calculations. Thus, the scissor operators are determined by the linear interpolation between the dielectric constants of AlN and AlP alloys, depending on the phosphorus content in the AlNP alloy. A similar method has been applied in previous works for calculating the energy band gaps of dilute-As AlNAs alloys.<sup>32</sup> Thus, the large reduction in the energy gap (~1.86 eV) of the  $\text{AlN}_{0.9375}\text{P}_{0.0625}$  alloy compared to AlN can be ascribed to the perturbations of the band structure caused by the introduction of defect P-states and may provide a new pathway for tuning the energy band gap in the AlN-based material system by tuning the P-content.

Figure 3 shows the energy band gaps and the corresponding emission wavelengths of the dilute-P AlNP alloys with P-content varying from 0% up to 6.25% obtained by DFT calculations. From figure 3, the energy band gap coverage of the dilute-P AlNP alloys shows a decreasing trend as more phosphorus is introduced into the system. Thus, the wavelength coverage found in this study spans from  $\lambda \sim 200$  nm up to  $\lambda \sim 290$  nm as the P-content is increased from 0% up to 6.25% in the AlNP alloy. This wavelength coverage provides excellent potential for the use of dilute-P AlNP alloys in mid and deep-UV photonic device applications. It should be noted that the strain effect was not taken into account in this work. It is expected that the  $\text{AlN}_{1-x}\text{P}_x$  alloys will require growth on non-native substrates like AlN. The biaxial strain induced during the growth would result in modifications of the band structure, in addition to the tensile strain that will result in further reduction of the effective band gap.<sup>41</sup> Moreover, it should be noted that although the trend in the energy band gap reduction is expected to mimic that of systems like the dilute-P GaNP alloys, there is no available literature for comparison on the electronic properties of dilute-P AlNP alloys up to present. Therefore, the understanding of the electronic and all other material properties of the dilute-P AlNP alloys is still at an early stage and the trends presented in this study will require further theoretical and experimental investigations.

Figure 4 presents the entire P-composition range of the AlNP alloys along with theoretical data for AlP from De and co-workers.<sup>42</sup> Note that the energy gap values are taken as the difference between the CBM and VBM and that the solid line in figure 4 is fitted based on the equation for the energy band gap  $E_g(x) = (1-x)E_{\text{AlN}} + (x)E_{\text{AlP}} + (1-x)(x)b$ , where  $b$  is defined as the bowing parameter. On the other hand, the dotted line in figure 4 represents the virtual crystal approximation (VCA) model, which excludes any bowing based on the P-content and is a linear interpolation between the AlN and AlP material systems. Our analysis indicates strong bowing in the AlNP alloy, in which the large bowing parameter reaches a value of  $28.3 \pm 0.5$  eV. Note that the AlP alloy band gap obtained from De and co-workers is a direct band gap semiconductor with a wurtzite crystal structure, which has not been demonstrated experimentally.<sup>42</sup> In addition, the AlNP alloys have not been experimentally realized either and the variations of the crystal structure as the P-concentration is increased is still unknown. Thus, the bowing parameter deduced in this work is only valid for dilute amounts of P-content in the

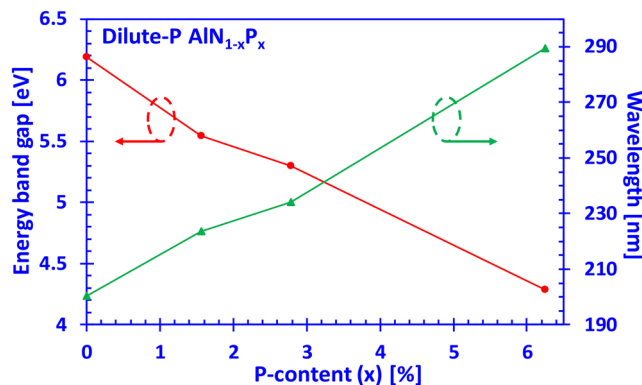


FIG. 3. Energy band gap values obtained through DFT calculations and the corresponding wavelength coverage of the dilute-P AlNP alloys for P-content from 0% up to 6.25%.

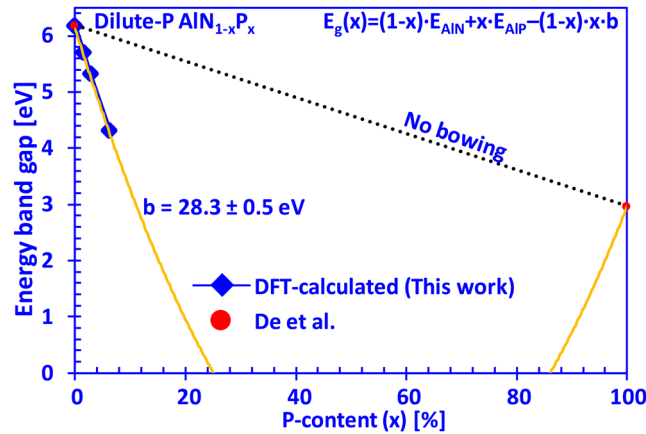


FIG. 4. Energy band gap values for the full P-composition range of the AlNP alloy based on the linear fitting of the DFT-data and corresponding bowing parameter  $b$ .

AlNP alloys (<10%) and further studies on the compositional dependence of the bowing parameter at higher P-content will be instrumental for a better understanding.

Figures 5(a) and 5(b) present the DFT-calculated lattice parameters for the dilute-P  $\text{AlN}_{1-x}\text{P}_x$  alloys with P-content up to 6.25%, for the  $a$  and  $c$  lattice constants, respectively. In addition, another set of lattice constants for comparison purposes in figures 5(a) and 5(b) are calculated from the linear interpolation of the lattice constants through the formulas  $a_{\text{AlNP}} = x \cdot a_{\text{AIP}} + (1-x) \cdot a_{\text{AlN}}$  and  $c_{\text{AlNP}} = x \cdot c_{\text{AIP}} + (1-x) \cdot c_{\text{AlN}}$ , respectively. Note that the AIP lattice constants used in the formulas are obtained from First-Principle data as the experimentally available data on wurtzite AIP crystals has not been reported.<sup>43</sup> Moreover, the  $a$  and  $c$  lattice constants obtained for AlN in this work are in excellent agreement with those published previously.<sup>44</sup> Thus, figures 5(a) and 5(b) indicate that the lattice constants of dilute-P AlNP alloys exhibit a linear increase with increasing the P-content, which can be attributed to the larger atomic size of the P-atoms as compared to the N-atoms. The increase in the lattice parameters in the dilute domain (<10%) is similar to III-nitride material systems InGaN, in which the difference in the atomic size lead to an increase in the lattice constants. On the other hand, the phenomenon shown in AlNP alloy is opposite to that of the dilute-N GaAsN system, where the N-atoms are smaller than the As-atoms and therefore lead to a decrease in the lattice constant.<sup>44,45</sup> Hence, the lattice parameters obtained in figures 5(a) and 5(b) will be essential in future device simulations employing this novel material system with minute phosphorus contents (<6.25%) in the dilute-P AlNP alloys.

Figure 6(a) and 6(b) indicate the carrier effective masses of dilute-P AlNP alloys with P-content ranging from 0% up to 6.25%, in the parallel ( $m_{\parallel}$ ) and perpendicular ( $m_{\perp}$ ) directions, respectively. The DFT-calculated band structures of the AlNP alloys were used to obtain the carrier effective

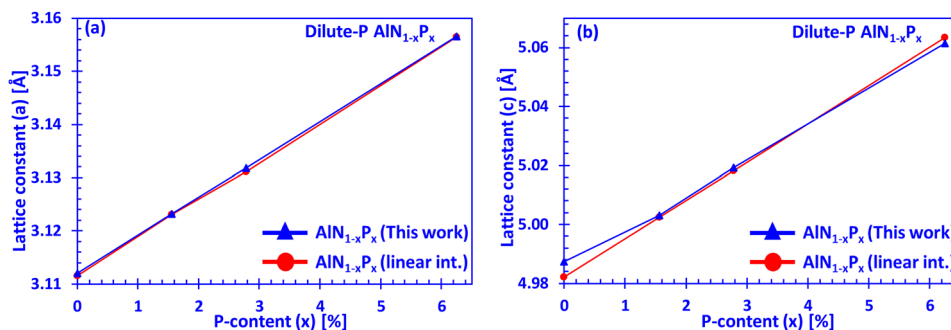


FIG. 5. Lattice parameters of dilute-P  $\text{AlN}_{1-x}\text{P}_x$  alloys for P-contents up to 6.25% obtained through DFT-calculations and linearly interpolated lattice parameters from experimental reports for the a)  $a$  and b)  $c$  lattice constants.

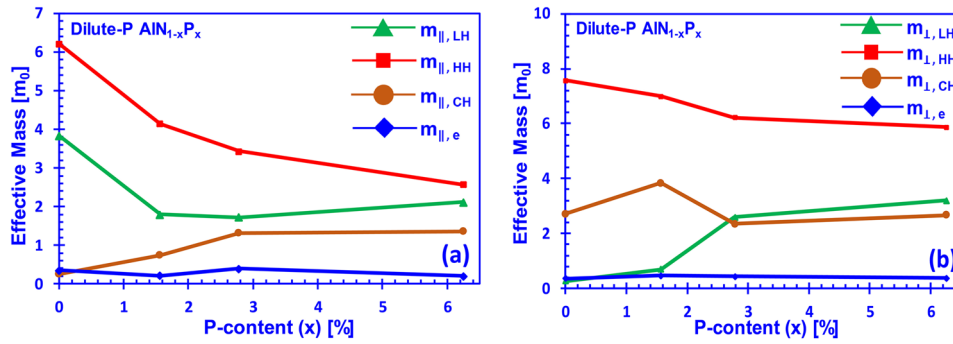


FIG. 6. Carrier effective masses of the light-hole (LH), heavy-hole (HH), crystal-field split-off (CH) bands and the electron, of the dilute-P  $\text{AlN}_{1-x}\text{P}_x$  alloys in the (a) parallel and (b) perpendicular directions.

masses by using the parabolic line fitting method. The carrier effective masses in the parallel and perpendicular directions near the gamma ( $\Gamma$ ) point were obtained by fitting the band dispersions of the  $\text{AlN}_{1-x}\text{P}_x$  alloys. The fittings to the energy band dispersions for the effective mass calculations were performed for small values (up to  $\sim 0.15$   $1/\text{\AA}$ ) of the  $\mathbf{k}$ -dependent wavevector in the parallel ( $\mathbf{k}_{\parallel}$ ) and perpendicular ( $\mathbf{k}_{\perp}$ ) directions. Thus, our findings on the values for the  $\mathbf{k}$ -dependent effective masses for AlN are in good agreement with values reported in the literature, where the values for the parallel (perpendicular) direction for the HH, LH, CH and electron effective masses are  $3.68$  ( $6.33$ )  $m_0$ ,  $3.68$  ( $0.25$ )  $m_0$ ,  $0.25$  ( $3.68$ )  $m_0$  and  $0.33$  ( $0.25$ )  $m_0$ , respectively.<sup>46</sup> Figure 6 shows that the HH and LH average effective masses are significantly perturbed with increasing the P-content in the  $\text{AlN}_{1-x}\text{P}_x$  alloys. Such behavior is likely to be attributed to the influence of the P-atoms on the valence band of the AlNP alloys, where similar phenomena have been observed for other dilute-anion III-nitride systems, like the dilute-P GaNP and dilute-As AlNAs alloys, where the effective masses of the heavy and light holes are largely perturbed.<sup>30,32</sup> On the other hand, the average effective mass of the electrons remains relatively unperturbed, while the  $m_{\parallel, \text{CH}}$  increases with increasing the P-content. Thus, the results presented in figure 6 may serve as guides for future experimental works as well as device simulations in the context of  $\mathbf{k} \cdot \mathbf{p}$  formalism employing the dilute-P  $\text{AlN}_{1-x}\text{P}_x$  material systems.

The state-of-the-art material system for use in active regions of III-nitride-based UV-regime photonic devices is currently the  $\text{Al}_x\text{Ga}_{1-x}\text{N}$  semiconductor, which has seen tremendous improvements in material synthesis quality as well as device-level engineering.<sup>9</sup> However, there still pertains the need to address the fundamental valence band crossover issue in AlGaN-based deep-UV light-emitting devices. The valence band crossover issue stems from the inherent property of high Al-content ( $>60\%$ ) AlGaN material system having the crystal-field split-off band (CH) positioned above the heavy-hole (HH) and light-hole (LH) bands. In the high Al-content case, the conduction band (C) to CH transitions will result in transverse-magnetic (TM) polarized light, making it difficult to extract light out of the quantum well as perpendicular light propagation is typically desired.<sup>17,18</sup> Thus, finding an alternative approach to tackle the fundamental valence band crossover issue in III-nitride-based photonic devices by achieving the dominant TE-polarized light emission is of high importance for future improvements targeting the deep-UV light-emitting devices.

In figure 7, the relative positions of the valence band edges (CH, HH and LH) of dilute-P AlNP alloys as a function of P-content ranging from 0% up to 6.25% are presented. The lines corresponding to each of the positions of the CH, HH and LH bands in figure 7 simply serve as indicators of the trend observed for the splitting of the CH and HH/LH bands as a function of P-content in the dilute-P AlNP alloys and should not be seen as absolute values for the valence subbands energies. Figure 7 indicates that the crossover of the CH and HH/LH bands occurs at  $\sim 1\%$  P-content, which is similar to previously reported values for the case of the dilute-As AlNAs alloys.<sup>32</sup> Accurate depiction of the absolute energy bands and their positions and the crossover phenomenon will require further studies involving experimental realization as well as more in-depth theoretical studies to understand the behavior of the valence bands of AlNP alloys due to minute additions of P-content. In addition,

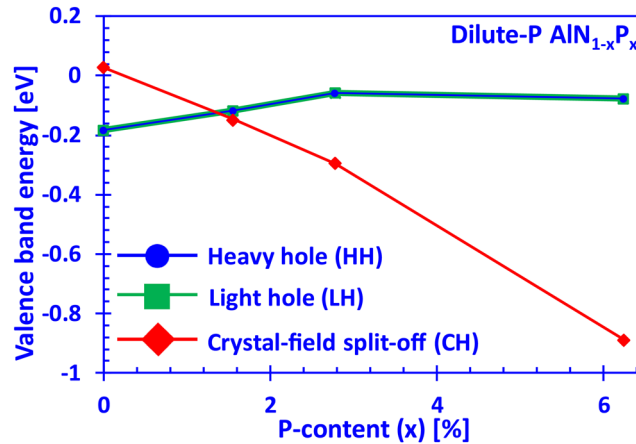


FIG. 7. Relative positions of the heavy-hole (HH), light-hole (LH) and crystal-field split-off (CH) bands of the dilute-P  $\text{AlN}_{1-x}\text{P}_x$  alloys.

the trends of the increasing separation of the HH/LH and CH bands as P-content is increased is similar to what has been previously reported in the highly-mismatched GaAsBi alloys, where higher Bi-content lead to a larger splitting of the valence bands and reduced energy band gap.<sup>47</sup> The findings in this work on the possibility of suppressing the fundamental valence band crossover issue and reducing the energy band gap in this AlN-based material system by incorporating small amounts of phosphorus are excellent motivation for future studies of this material system, as it may pave a new pathway for achieving highly-efficient III-nitride-based deep-UV devices with TE-dominant polarization in the future.

#### IV. CONCLUSIONS

In summary, the electronic properties of the novel dilute-P  $\text{AlN}_{1-x}\text{P}_x$  alloys have been investigated by the means of First-Principle DFT calculations, where the P-content was varied from 0% up to 6.25%. The analysis indicates that the novel dilute-P AlNP alloys exhibit the direct band gap property and that the energy band gap coverage ranges from 6.19 eV (0% P-content) down to 4.32 eV (6.25% P-content). This large band gap reduction indicates a possibility of using the dilute-P AlNP alloys for applications in the wavelength regime spanning from  $\lambda \sim 200$  nm up to  $\lambda \sim 290$  nm, allowing access to the deep-UV regime. Additionally, the lattice parameters  $a$  and  $c$  of dilute-P AlNP alloys were presented and results were compared to previous reports on AlN as well as linearly interpolated lattice constants between AlN and AlP in the wurtzite crystal structure. Our findings indicate a large bowing parameter of  $b = 28.3 \pm 0.5$  eV with the introduction of minute amounts of phosphorus. Moreover, the average carrier effective masses of the dilute-P AlNP alloys by using parabolic line fitting are presented. The analysis also extends to elaborate on the potential of using the dilute-P AlNP alloys for addressing the valence band crossover issue in AlN-based alloys by inserting very dilute amounts of phosphorus ( $\sim 1$ -2%) into the AlNP system. Namely, the TE-dominant polarization where the heavy-hole and light-hole valence subbands are positioned above the crystal-field split-off band occurs at very low P-content ( $\sim 1\%$ ), providing a potential new method to overcome this issue in AlN-based heterostructures for UV emission. Thus, the electronic properties of dilute-P AlNP alloys presented in this work shed light on their promising fundamental properties required for considering them as potential candidates for implementation in future photonic devices operating in the and deep-UV wavelength regimes.

#### ACKNOWLEDGMENTS

The work is supported by US National Science Foundation (DMR 1505122 and ECCS 1408051), and the Daniel E. '39 and Patricia M. Smith Endowed Chair Professorship Fund.

- <sup>1</sup> S. Nakamura and G. Fasol, (Eds.), *The Blue Laser Diode*, (Springer-Verlag, Berlin 1997).
- <sup>2</sup> H. Harima, *J. Phys.: Condens. Matter* **14**, R967–R993 (2002).
- <sup>3</sup> G. Zeng, C. K. Tan, N. Tansu, and B. A. Krick, *Appl. Phys. Lett.* **109**, 051602 (2016).
- <sup>4</sup> M. H. Crawford, *IEEE J. Sel. Top. Quantum Electron.* **15**, 1028–1040 (2009).
- <sup>5</sup> V. Cimalla, J. Pezoldt, and O. Ambacher, *J. Phys. D: Appl. Phys.* **40**, 6386 (2007).
- <sup>6</sup> U. K. Mishra, L. Shen, T. E. Kazior, and Y. F. Wu, *Proc. IEEE* **96**, 287 (2008).
- <sup>7</sup> E. F. Schubert, *Light-Emitting Diodes* (Cambridge University Press, 2006).
- <sup>8</sup> [http://www.nobelprize.org/nobel\\_prizes/physics/laureates/2014](http://www.nobelprize.org/nobel_prizes/physics/laureates/2014).
- <sup>9</sup> K. Ding, V. Avrutin, Ü. Özgür, and H. Morkoç, *Crystals* **7**, 300 (2017).
- <sup>10</sup> T. Takano, T. Mino, J. Sakai, N. Noguchi, K. Tsubaki, and H. Hirayama, *Appl. Phys. Express* **10**, 3 (2017).
- <sup>11</sup> Y. Narukawa, M. Ichikawa, D. Sanga, M. Sano, and T. Mukai, *J. Phys. D* **43**, 354002 (2010).
- <sup>12</sup> M. Shatalov, W. Sun, A. Lunev, X. Hu, A. Dobrinsky, Y. Bilenko, J. Yang, M. Shur, R. Gaska, C. Moe, G. Garrett, and M. Wraback, *Appl. Phys. Express* **5**, 082101 (2012).
- <sup>13</sup> H. Hirayama, T. Takano, J. Sakai, T. Mino, K. Tsubaki, N. Maeda, M. Jo, Y. Kanazawa, I. Ohshima, T. Matsumoto, and N. Kamata, Proc. of the 2016 International Semiconductor Laser Conference (ISLC), pp. 1-2, September 12-15 (2016).
- <sup>14</sup> S.-I. Inoue, T. Naoki, T. Kinoshita, T. Obata, and H. Yanagi, *Appl. Phys. Lett.* **106**, 131104 (2015).
- <sup>15</sup> A. Fujioka, K. Asada, H. Yamada, T. Ohtsuka, T. Ogawa, T. Kosugi, D. Kishikawa, and T. Mukai, *Semiconductor Science and Tech.* **29**, 8 (2014).
- <sup>16</sup> M. Kneissl, T. Kolbe, C. Chua, V. Kueller, N. Lobo, J. Stellmach, A. Knauer, H. Rodriguez, S. Einfeldt, Z. Yang, N. M. Johnson, and M. Weyers, *Semiconductor Science and Tech.* **26**, 014036 (2011).
- <sup>17</sup> H. Kawanishi, E. Niikura, M. Yamamoto, and S. Takeda, *Appl. Phys. Lett.* **89**, 251107 (2006).
- <sup>18</sup> J. Zhang, H. P. Zhao, and N. Tansu, *Appl. Phys. Lett.* **97**, 111105 (2010).
- <sup>19</sup> J. J. Wierer, D. A. Steigerwald, M. R. Krames, J. J. O'Shea, M. J. Ludowise, G. Christenson, Y.-C. Shen, C. Lowery, P. S. Martin, S. Subramanya, W. Götz, N. F. Gardner, R. S. Kern, and S. A. Stockman, *J. Appl. Phys. Lett.* **78**, 22 (2001).
- <sup>20</sup> K. Tadatomo, H. Okagawa, Y. Ohuchi, T. Tsunekawa, Y. Imada, M. Kato, and T. Taguchi, *Jpn. J. Appl. Phys.* **40**, 6B (2001).
- <sup>21</sup> S. Yoshida, J. Kikawa, and Y. Itoh, *J. Crystal Growth* **237-239**, 1037–1041 (2002).
- <sup>22</sup> A. Kimura, C. A. Paulson, H. F. Tang, and T. F. Kuech, *Appl. Phys. Lett.* **84**(9), 1489–1491 (2004).
- <sup>23</sup> S.-H. Moon, H.-A. Do, J. Park, and S.-W. Ryu, *Journal of Materials Research* **24**(12), 3569–3572 (2009).
- <sup>24</sup> L. Zhang, H. F. Tang, J. Schieke, M. Mavrikakis, and T. F. Kuech, *Jour. of Crystal Growth* **242**, 302–308 (2002).
- <sup>25</sup> R. A. Arif, H. P. Zhao, and N. Tansu, *Appl. Phys. Lett.* **92**, 011104 (2008).
- <sup>26</sup> C. K. Tan, D. Borovac, W. Sun, and N. Tansu, *Sci. Rep.* **6**, 19271 (2016).
- <sup>27</sup> D. Borovac, C. K. Tan, and N. Tansu, *Sci. Rep.* **7**, 17285 (2017).
- <sup>28</sup> C. K. Tan, J. Zhang, X. H. Li, G. Liu, B. O. Tayo, and N. Tansu, *J. Disp. Tech.* **9**(4), 272–279 (2013).
- <sup>29</sup> C. K. Tan and N. Tansu, *AIP Advances* **5**(5), 057135 (2015).
- <sup>30</sup> C. K. Tan, D. Borovac, W. Sun, and N. Tansu, *Sci. Rep.* **6**, 24412 (2016).
- <sup>31</sup> T. Takayama, M. Yuri, K. Itoh, and J. S. Harris, Jr., *J. Appl. Phys.* **90**, 2358–2369 (2001).
- <sup>32</sup> C. K. Tan, D. Borovac, W. Sun, and N. Tansu, *Scientific Reports* **6**, 22215 (2016).
- <sup>33</sup> V. Fiorentini and A. Baldereschi, *Phys. Rev. B, Condens. Matter* **51**, 23 (1995).
- <sup>34</sup> G. Kresse and J. Hafner, *Phys. Rev. B* **47**, 55 (1993).
- <sup>35</sup> G. Kresse and J. Hafner, *Phys. Rev. B* **49**, 14251 (1994).
- <sup>36</sup> G. Kresse and J. Furthmüller, *Comput. Mat. Sci.* **6**, 15 (1996).
- <sup>37</sup> G. Kresse and J. Furthmüller, *Phys. Rev. B* **54**, 11169 (1996).
- <sup>38</sup> J. P. Perdew, K. Burke, and M. Ernzerhof, *Phys. Rev. Lett.* **77**, 18 (1996).
- <sup>39</sup> T. Mattila and A. Zunger, *Phys. Rev. B* **58**, 1367–1373 (1998).
- <sup>40</sup> W. M. Yim, E. J. Stofko, P. J. Zanzucchi, J. I. Pankove, M. Ettenberg, and S. L. Gilbert, *Jour. of Applied Phys.* **44**, 292 (1973).
- <sup>41</sup> W. Shan, R. J. Hauenstein, A. J. Fischer, J. J. Song, W. G. Perry, M. D. Bremser, R. F. Davis, and B. Goldenberg, *Phys. Rev. B* **54**, 13460 (1996).
- <sup>42</sup> A. De and C. E. Pryor, *Phys. Rev. B* **81**, 155210 (2010).
- <sup>43</sup> C. Y. Yeh, Z. W. Lu, S. Froyen, and A. Zunger, *Phys. Rev. B* **46**, 16 (1992).
- <sup>44</sup> I. Vurgaftman and J. R. Meyer, *J. Appl. Phys.* **94**, 3675–3696 (2003).
- <sup>45</sup> W. Li, M. Pessa, and J. Likonen, *Appl. Phys. Lett.* **78**, 2864 (2001).
- <sup>46</sup> M. Suzuki and T. Uenoyama, *Phys. Rev. B* **52**, 8132–8139 (1995).
- <sup>47</sup> Z. Batool, K. Hild, T. J. C. Hosea, X. Lu, T. Tiedje, and S. J. Sweeney, *J. of Appl. Phys.* **111**, 113108 (2012).